LLaTTE: Scaling Laws for Multi-Stage Sequence Modeling in Large-Scale Ads Recommendation

Lee Xiong[†], **Zhirong Chen**[†], **Rahul Mayuranath**[†], **Shangran Qiu**, **Arda Ozdemir**, **Lu Li**, **Yang Hu**, **Dave Li**, **Jingtao Ren**, **Howard Cheng**, **Fabian Souto Herrera**, **Ahmed Agiza**, **Allen Lin**, **Baruch Epshtein**, **Anuj Aggarwal**, **Julia Ulziisaikhan**, **Chao Wang**, **Dinesh Ramasamy**, **Parshva Doshi**, **Sri Reddy**, **Arnold Overwijk**

[†]First Authors, AI at Meta

We present **LLaTTE** (LLM-Style Latent Transformers for Temporal Events), a scalable transformer architecture for production ads recommendation. Through systematic experiments, we demonstrate that sequence modeling in recommendation systems follows predictable power-law scaling similar to LLMs. Crucially, we find that semantic features *bend the scaling curve*: they are a prerequisite for scaling, enabling the model to effectively utilize the capacity of deeper and longer architectures. To realize the benefits of continued scaling under strict latency constraints, we introduce a two-stage architecture that offloads the heavy computation of large, long-context models to an asynchronous upstream user model. We demonstrate that upstream improvements transfer predictably to downstream ranking tasks. Deployed as the largest user model at Meta, this multi-stage framework **drives a 4.3% conversion uplift on Facebook Feed and Reels** with minimal serving overhead, establishing a practical blueprint for harnessing scaling laws in industrial recommender systems.

∞ Meta

1 Introduction

The convergence of sequence modeling and recommendation systems has opened new frontiers in artificial intelligence. Modern recommendation systems, particularly in advertising and content platforms, process billions of user interactions daily as each user's journey through products, ads, and content forms a rich temporal sequence that encodes user preferences and intent. While Large Language Models (LLMs) have demonstrated that deep sequence models can achieve remarkable performance through predictable scaling laws Kaplan et al. (2020) (with capabilities improving as power-law functions of model size, data, and compute), production recommendation systems have largely remained constrained to shallower sequence architectures Kang and McAuley (2018); Sun et al. (2019); Chen et al. (2019).

This gap persists despite the sequential nature of user behavior and the potential for similar scaling benefits. The challenges are twofold: (i) reconciling the computational demands of deep sequence models with the strict latency requirements of production serving, where systems must rank hundreds of candidates within milliseconds, and (ii) bridging the architectural divide between traditional Factorization Machine (FM) based models Zhang et al. (2024b) and transformer-based sequence models. FM-based models excel at learning from massive sparse and dense feature spaces (user IDs, item IDs, request and contextual features), but they lack sequential modeling capacity, while sequence models capture temporal dynamics but struggle to efficiently incorporate the high-dimensional non-sequence features critical for production performance. Understanding

how to effectively scale sequence models while preserving the strengths of both paradigms under production constraints, and harness predictable scaling laws in this hybrid regime, remains a challenge that bridges research and real-world deployment.

To address these challenges, we structured our investigation around three research questions: **RQ1**, How can we design sequence models that integrate with FM-based architectures to leverage both sparse collaborative signals and temporal dynamics? **RQ2**, Do recommendation systems exhibit predictable scaling behaviors similar to LLMs, with identifiable trade-offs, capacity bottlenecks, and data quality impacts? **RQ3**, How can we harness scaling benefits while meeting strict production latency requirements?

We introduce **LLaTTE** (LLM-Style Latent Transformers for Temporal Events), an architectural paradigm deployed in our massive-scale production systems that addresses all three questions. LLaTTE enables efficient scaling through two key innovations that reconcile deep sequence modeling with our production constraints:

1. **Target-Aware Adaptive Transformer**: Our sequence module integrates non-sequence sparse features and candidate information into extended query tokens, leveraging Multi-head Latent Attention (MLA) DeepSeek-AI (2024). The architecture supports adaptive pyramidal output extraction, which can optionally be employed to progressively reduce computational complexity. This design seamlessly integrates with FM-style modules, enabling us to harness the scaling gains of deep sequence processing within strict production inference budgets.

1

2. **Multi-Stage Architecture**: To harvest scaling benefits under strict latency constraints, we introduce an **upstream** stage that runs large LLaTTE encoders, triggered by high-value user events, to asynchronously generate and cache compressed user embeddings that are not bounded by request-time latency. The **online** ranking stage combines these cached embeddings with fresh, short-horizon sequential signals processed by a lightweight LLaTTE counterpart. Both stages share a common sequence architecture while operating at drastically different scales. Specifically, the upstream model consumes $> 45\times$ the sequence FLOPs of its online counterpart. This asymmetry allows us to offload the vast majority of sequence computation without impacting online serving latency.

Through systematic experiments spanning model depth, width, sequence length, data enrichment via content understanding model features, and cross-stage transfer dynamics, we provide comprehensive answers to foundational scaling behavior questions in the recommendation system setting, revealing several key insights: (i) Performance follows predictable log-linear scaling laws, with sequence length serving as a primary lever; (ii) Data enrichment such as semantic content embeddings is not merely additive but a *prerequisite* for steeper scaling curves, effectively bending the scaling laws beyond what sparse ID signals allow; (iii) Improvements from upstream modeling transfer predictably to online ranking stages with a high transfer ratio ($\approx 50\%$), validating the efficacy of our multi-stage design even across a strict information bottleneck; and (iv) Model width acts as a capacity bottleneck; sufficient width must be established before depth scaling becomes effective. These findings establish that recommendation systems can benefit from scaling laws analogous to LLMs when architectural constraints are properly addressed.

Our production deployment validates these findings, demonstrating that the two-stage architecture achieves a **0.25%** improvement in Normalized Entropy on our primary revenue-generating models with minimal serving overhead. Together, our architectural innovations and empirical scaling laws provide a systematic framework for scaling sequence models in large-scale production recommendation systems.

2 Background and Related Work

Our work intersects three research areas: transformer-based sequence modeling in recommendation systems, scaling laws for neural networks, and multi-stage architectures for production deployment. We review each area and position our contributions.

2.1 Sequence Modeling in Recommendation

Early sequential recommendation approaches used recurrent neural networks for modeling sequential behavior. GRU4Rec Hidasi et al. (2016) pioneered RNNs for session-based recommendation, followed by various LSTM variants Donkers et al. (2017). The introduction of self-attention mechanisms marked a significant advance in the field. SASRec Kang and McAuley (2018) and HLLM Chen et al. (2024) applied self-attention to next-item prediction, enabling parallel processing and better long-range modeling. BERT4Rec Sun et al. (2019) adapted bidirectional transformers using masked item prediction, while S3-Rec Zhou et al. (2020) introduced self-supervised pretraining for sequential recommendation.

Target-aware attention mechanisms have also proven critical for production CTR prediction. DIN Zhou et al. (2018) introduced attention weighted by the target item, later extended by DIEN Zhou et al. (2019) with interest evolution modeling.

Recent work has explored different architectural choices for integrating sequential and non-sequential features. HSTU Zhai et al. (2024), OneTrans Zhang et al. (2025), and LONGER Chai et al. (2025) advocate for pure sequence-based architectures, while InterFormer Zeng et al. (2025) proposes interleaving sequence and non-sequence computation at each layer. However, these approaches require tight coupling to specific architectures, limiting flexibility for independent scaling of sequence modules and preventing easy separation of model inference across online and offline stages. This architectural rigidity has constrained production systems to relatively small sequence models processing limited context.

2.2 Scaling Laws

Kaplan et al. Kaplan et al. (2020) demonstrated that language model performance follows power-law relationships with model size, dataset size, and compute budget. While recent work has explored scaling in recommender systems Zhang et al. (2025, 2024b), these studies typically examine either individual scaling dimensions in isolation or their compounding effects, without systematically investigating how different scaling axes interact. Moreover, they overlook critical dimensions such as data richness and composition, which are particularly important for large-scale production recommendation systems. We address this by modeling the joint interaction of depth, width, and feature richness, identifying critical thresholds where scaling behavior fundamentally shifts.

2.3 Multi-Stage Architectures in Production RecSys

Multi-stage architectures, which separate representation learning from task-specific prediction, have emerged as a practical paradigm for modeling in production recommendation systems. These approaches aim to balance model expressiveness with the stringent latency requirements of online serving.

Embedding-based approaches precompute user representations for consumption by online ranking models. Pinnerformer Pancha et al. (2022) learns user embeddings from sequential engagement data using a transformer trained with a

dense all-action loss over engagement windows. SUM Zhang et al. (2024a) provides a framework for sharing user representations across hundreds of production models via asynchronous inference. Both systems decouple upstream computation from online serving, enabling larger models than real-time latency budgets would permit.

TransAct Xia et al. (2023) introduces a hybrid architecture that combines precomputed embeddings with real-time processing of recent user actions. The system processes recent actions ($O(10^2)$) through a transformer while leveraging precomputed embeddings for long-term interests. TransAct V2 Xia et al. (2025) extends the real-time component to longer sequences ($O(10^4)$) using candidate-anchored nearest neighbor search and custom GPU kernels.

An alternative approach uses retrieval-based designs that operate synchronously within each request. SIM Pi et al. (2020) introduced the GSU-ESU paradigm, where a General Search Unit retrieves relevant behaviors before an Exact Search Unit applies target-aware attention. TWIN Chang et al. (2023) improves consistency between stages by ensuring both use identical relevance metrics, scaling to 10^4–10^5 behaviors at Kuaishou. TWIN V2 Si et al. (2024) extends to lifecycle-scale sequences through hierarchical clustering compression.

Despite these advances, prior multi-stage work has not explored systematic model scaling following predictable scaling laws. These systems typically scale along a single dimension (e.g., sequence length in TransAct V2) while keeping models relatively small overall. In this work, we show that a unified scaling framework applies to both real-time and asynchronous upstream ranking settings. We systematically examine how increasing model capacity across multiple dimensions and allocating capacity between online and upstream stages, affects performance in production recommendation systems. To our knowledge, this is the first work to establish empirical scaling laws for such hybrid upstream-downstream architectures. Additionally, we rigorously quantify the *transfer ratio* between stages, offering a metric to measure how effectively scaling laws traverse the inference bottleneck.

3 Preliminaries: Ads Recommendation Stack

We consider a standard multi-task ads ranking problem where the model predicts engagement probabilities such as click-through rate (CTR) and conversion rate (CVR). These calibrated probabilities are utilized for both downstream ranking and auction pricing.

Task   Given a user u, candidate ad i, and request context c, the model predicts a vector of engagement probabilities:

$$\mathbf{y} = f(\mathbf{x}_u, \mathbf{x}_i, \mathbf{x}_{ui}, \mathbf{x}_c; \boldsymbol{\theta}) \in [0, 1]^{|\mathcal{H}|}, \quad (1)$$

where $\mathcal{H} = \{\text{CTR}, \text{CVR}, \dots\}$ is the set of prediction heads and $\boldsymbol{\theta}$ denotes model parameters.

Feature Structure   We categorize input features along two axes. By **source**, we distinguish: (1) **User** $\mathbf{x}_u$ (demographics, aggregates, behavioral sequence S_u); (2) **Ad** $\mathbf{x}_i$ (creative attributes, landing page, advertiser metadata); (3) **User-Ad** $\mathbf{x}_{ui}$ (historical interactions); and (4) **Context** $\mathbf{x}_c$ (time, device, surface).

By **type**, features are processed as:

- **Sparse IDs** $\mathbf{x}_{\text{sparse}} \in \mathcal{V}^{m_{\text{sparse}}}$: categorical entities mapped to embeddings.
- **Dense features** $\mathbf{x}_{\text{dense}} \in \mathbb{R}^{m_{\text{dense}}}$: precomputed embeddings (e.g., from content encoders).
- **Float attributes** $\mathbf{x}_{\text{float}} \in \mathbb{R}^{m_{\text{float}}}$: continuous variables.
- **Sequences** S_u: ordered lists of temporal events.

User Sequences   User behavioral sequence $S_u = \{a_1, a_2, \dots, a_T\}$ is a temporally ordered list of actions. Each action a_t consists of a timestamp, action type, item identifier, surface type, optional content embeddings and other metadata. In our experiments, sequence lengths T range from 500 to 5000 actions.

Objective and Evaluation   We train using a weighted multi-task binary cross-entropy loss. Our primary evaluation metric is the relative improvement in *Normalized Entropy* (NE). NE is defined as the average log loss normalized by the entropy of the empirical CTR:

$$\text{NE} = \frac{-\frac{1}{N} \sum_{i=1}^{N} \left[y_i \log \hat{y}_i + (1 - y_i) \log(1 - \hat{y}_i) \right]}{-\left[p \log p + (1 - p) \log(1 - p) \right]}, \quad (2)$$

where p is the empirical positive rate observed from the ground truth. NE is a standard metric in industrial recommendation.

4 Experimental Backbone: The LLaTTE Paradigm

To systematically study scaling laws in recommendation, we require an architecture that is both representative of modern production systems and efficient enough to scale to massive contexts. We adopt a modular design, referred to as **LLaTTE** (LLM-Style Latent Transformers for Temporal Events), that synthesizes best practices in efficient sequence modeling.

The architecture (Figure 1) consists of three components: (i) a **Sequence Module** that encodes user behavioral histories; (ii) a **Non-Sequence Module** that integrates sequence summaries with static features; and (iii) **Task Heads** for prediction.

Compute Allocation. In our production setting, the sequence module accounts for over 90% of total inference FLOPs in
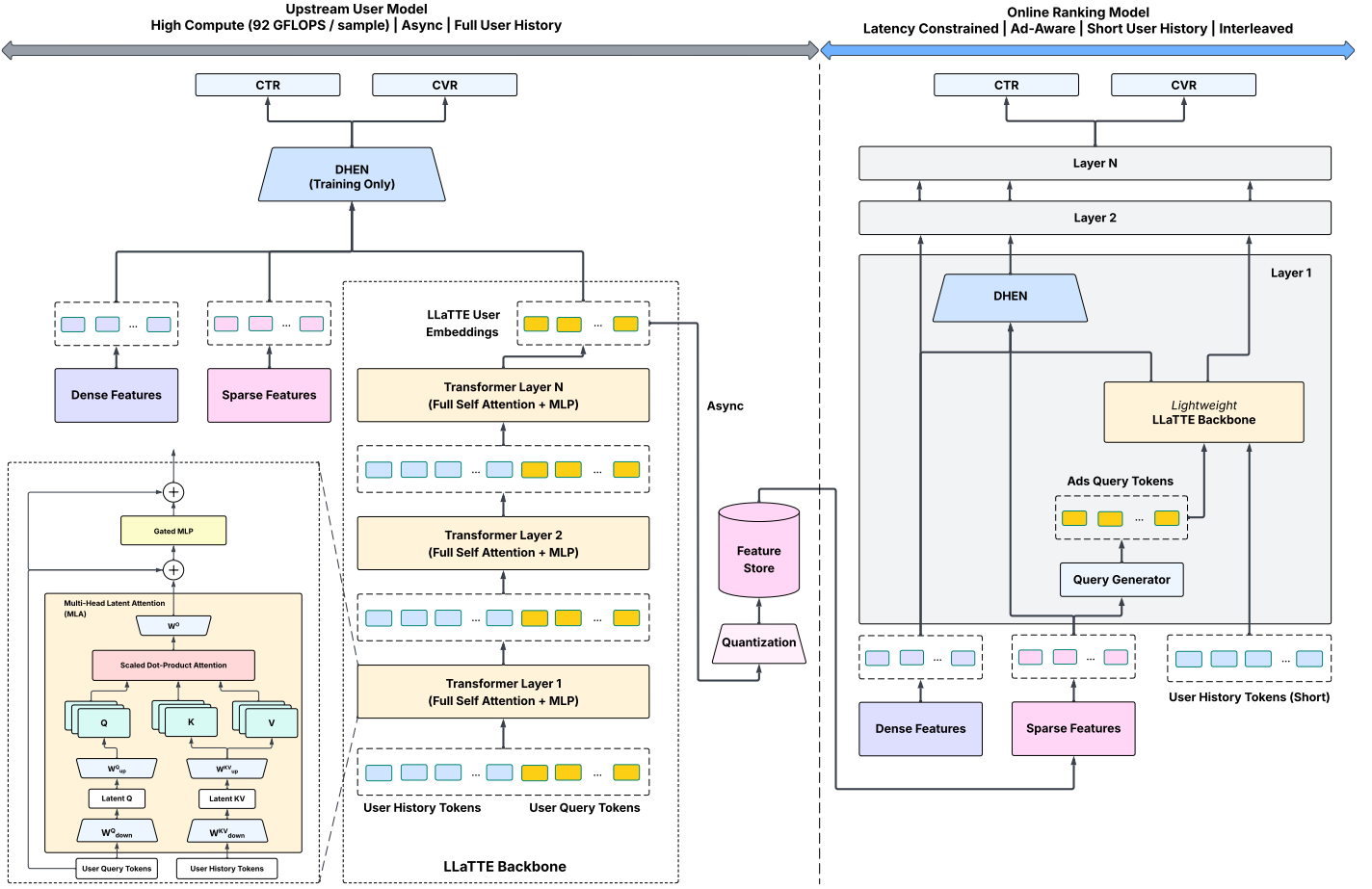
Figure 1 LLaTTE architecture overview. We hold the non-sequence backbone (DHEN) and task heads fixed, and scale the transformer-based sequence module in depth, width, and sequence length. The sequence module utilizes Multi-head Latent Attention (MLA) and adaptive pyramidal trimming to efficiently process long user histories.

the large-scale **upstream** model, while a lightweight sequence module counterpart accounts for roughly 30% of the **online** ranking model FLOPs. In subsequent scaling experiments, we focus our study on the large-scale upstream model by default, where varying the capacity (L, d, T) of the Sequence Module allows us to explore scaling behaviors across a much wider compute FLOP range than is possible with the lightweight online ranking model. The Non-Sequence backbone and Task Heads are held fixed throughout to isolate the effects of Sequence Module scaling.

4.1 Non-Sequence Backbone

The non-sequence module implements a standard DHEN-style architecture Zhang et al. (2022), a deep ensemble network that combines heterogeneous feature interaction modules. It processes all non-sequential features alongside the sequence summaries $\mathbf{z}_{\text{seq}}^{(k)}$ produced by the transformer.

Sparse categorical features are embedded and concatenated with dense/float features. The concatenated features are passed through L_{NS} layers of feature interaction networks to yield a unified representation $\mathbf{z}$. Prediction heads are

shallow MLPs producing probabilities $\hat{y}_h = \sigma(\text{MLP}_h(\mathbf{z}))$.

4.2 Sequence Module

The sequence module is the focus of our scaling study. To enable scaling to long contexts (lengths > 1000) under production constraints, we employ a **Target-Aware** transformer with two key efficiency optimizations: **Multi-head Latent Attention (MLA)** and **Adaptive Pyramidal Output**.

The module operates in five steps:

1. **Tokenization:** Embeds each action a_t into a token vector $\mathbf{x}_t$, forming $\mathbf{X}_{\text{seq}}$.
2. **Fusion:** Appends n_q query tokens to form $\mathbf{X}_{\text{input}}$. We encode the query tokens with user-ad candidate context for online model, and user-only context for upstream model when ad candidate context isn't available yet. This flexible encoding allows the same architecture to bridge offline and online stages.
3. **Latent Attention:** Applies an L-layer transformer using MLA DeepSeek-AI (2024) to reduce memory footprint.
4. **Pyramidal Reduction:** Selectively trims older tokens at

4

deeper layers (following Zhang et al. (2025)). This concentrates compute on recent events and query tokens, allowing the model to trade off context length against FLOPs.

5. **Readout:** Extracts fixed-size summaries from the final query-token representations.

This adaptive design allows us to deploy different flavors of LLaTTE across the stack while maintaining a unified modeling paradigm. In the asynchronous **upstream** stage, we deploy high-capacity variants that consume $> 45\times$ **the sequence FLOPs** of the main ranker (with $> 90\%$ concentrated in the Sequence Module), utilizing full self-attention to maximize representation quality. Conversely, **online** ranking models employ aggressive pyramidal trimming to adhere to strict latency budgets. The architecture composes standardized components; full specifications appear in Appendix A.

5 Scaling Framework and Methodology

To rigorously quantify the benefits of scaling in recommendation, we move beyond ad-hoc architecture search and adopt a systematic scaling framework. Unlike LLMs, where the input text distribution is generally treated as fixed, recommendation systems allow us to scale along both architectural dimensions and input information densities.

We formulate the scaling behavior as a function of the compute budget $\mathcal{C}$, measured in FLOPs allocated to the sequence module. When the information density is held constant, we posit that Normalized Entropy (NE) improvements (relative to our strong production baseline) follow a power-law relationship with compute, modeled log-linearly as:

$$\Delta\mathrm{NE}(\mathcal{C}) \propto -\alpha \cdot \log_{10} \mathcal{C} \tag{3}$$

where α represents the scaling coefficient (efficiency) of a specific dimension. We investigate four primary axes of scaling:

1. Model Capacity (L, d). We vary the transformer depth L and embedding width d. A key objective is to identify the *aspect ratio L/d* that maximizes parameter efficiency, determining if critical width thresholds exist before depth scaling becomes effective in the sparse-feature regime of recommendation systems.

2. Temporal Horizon (T). We treat sequence length T as a direct proxy for the information horizon. We examine if extending T yields diminishing returns or if larger models can effectively attend to increasingly distant history events $(T \to 5000)$.

3. Information Density. Standard scaling laws assume a homogeneous token distribution. We challenge this by varying the semantic richness of the tokens $\mathbf{x}_t$. We compare sparse ID-based tokens against tokens enriched with dense semantic embeddings from foundational content encoders, treating *signal quality* as a multiplier on the scaling coefficient α.

4. Cross-Stage Transfer Efficiency. To quantify cross-stage efficiency, we introduce the **Transfer Ratio** (τ) which measures how effectively improvements from a large upstream model translate to the production online ranking loss. This metric accounts for all production interference factors such as asynchronous inference latency penalties.

$$\tau = \frac{\Delta\mathrm{NE}_{\mathrm{downstream}}}{\Delta\mathrm{NE}_{\mathrm{upstream}}} \tag{4}$$

where $\Delta\mathrm{NE}_{\mathrm{upstream}}$ is the loss reduction in the offline user modeling task and $\Delta\mathrm{NE}_{\mathrm{downstream}}$ is the realized gain in the online ranking task. This metric allows us to determine which scaling axes best preserve gains through the information bottleneck inherent in multi-stage architectures.

6 Experimental Results

6.1 Experimental Setup

Training infrastructure. All scaling experiments are conducted on the same large-scale production recommendation task using a proprietary industrial training platform. As previously noted, our experiments are conducted on the large upstream model to investigate the maximum achievable FLOP horizon, extending beyond the computational limits of the online model. Models are trained with mixed precision on **128** NVIDIA H100 GPUs and use FlashAttention Dao et al. (2022) for memory and throughput efficiency. Unless otherwise noted, each configuration is trained for **229K** steps on **30 billion** examples sampled from the production traffic distribution.

Evaluation metric. We report all results using *Normalized Entropy* (NE), defined in Eq. 2. We report relative reductions in NE (%) compared to a strong production baseline, where lower NE values indicate better performance. On our internal datasets, a reduction in NE of **0.02%** is considered statistically significant and sufficient to yield measurable revenue impact.

6.2 Scaling Model Depth and Width

We first investigate how to allocate a fixed compute budget between model depth (L) and width (d). We conduct a grid search over $L \in \{1, 2, 4, 8\}$ and $d \in \{128, 256, 512, 1024\}$ at a fixed sequence length of $T = 400$.

The results reveal a non-linear relationship between depth and width. When the model is narrow $(d = 128)$, increasing depth yields diminishing returns; the representation capacity is bottlenecked by the embedding dimension. However, once width reaches a critical threshold of $d \approx 256$, depth scaling becomes substantially more effective. Conversely, allocating

compute purely to width (fixing L and increasing $d \rightarrow 1024$) yields limited NE gains.

To illustrate these regimes, Table 1 compares four representative configurations. We include a "Deep-Balanced" variant to demonstrate the scaling behavior when both depth and width are sufficient. Extreme or unbalanced allocation to either width or depth leads to diminishing returns. Sufficient width ($d \geq 256$) is required for depth scaling to be effective, while excessive width without adequate depth (e.g., $d = 1024$) is computationally inefficient and yields limited gains. Balanced configurations maximize performance and compute efficiency.

Table 1 Capacity allocation across depth and width. **Deep-Balanced** ($d = 256$) successfully leverages depth to achieve the best performance (-0.17%)

Setting	Deep Narrow	Balanced	Deep Balanced	Shallow Wide
Depth (L)	8	4	8	2
Width (d)	128	256	256	1024
Seq Params (M)	0.85	1.16	2.33	6.93
Seq FLOPs (M)	568	**530**	1187	1909
NE △ (%)	-0.10%	-0.14%	**-0.17%**	-0.08%

Motivated by these observations, we adopt balanced configurations ($d \geq 256$) as the default when studying other scaling axes such as sequence length and content features.

6.3 Sequence Length, Composition, and Content

We now examine how LLaTTE performance scales with the temporal horizon proportional to the number of events T, and with the semantic content embeddings on each event.

6.3.1 Extending the temporal horizon

We vary the sequence horizon $T \in \{200, 400, 800, 1600\}$ for models with depths $L \in \{1, 2, 4, 8\}$ while keeping width fixed. As summarized in Figure 2, NE decreases monotonically with T across all depths, confirming that longer user histories consistently improve ranking quality.

The incremental benefit of additional context depends strongly on model capacity. Deeper models exhibit larger NE gains as T increases, which is reflected in the curves for $L = 2$ compared to $L = 1$ in Figure 2.

Attention-score probability analyses also revealed the utility of long contexts. The cumulative attention probability distributions over positions (Figure 3) show that a non-trivial fraction of attention probability is allocated across the entire 200–1600 token range, rather than narrowly focusing on the most recent events, indicating that mid- and long-range history contributes meaningfully to predictions. The details of this study can be found in the Appendix (see Section A.4).
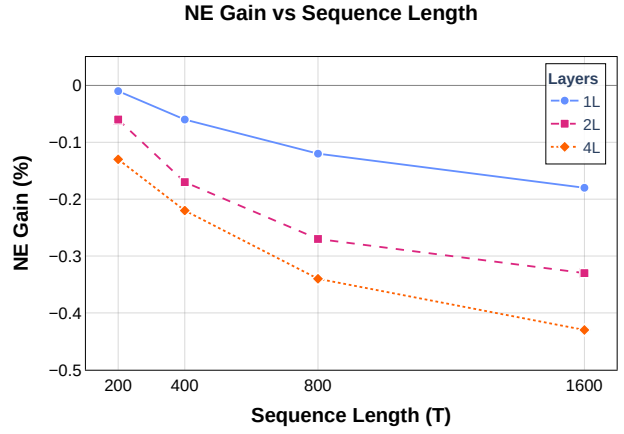

Figure 2 Sequence length scaling for $L = 1$, $L = 2$, and $L = 4$ models. NE improves smoothly with longer histories, with deeper models exhibiting a steeper dependence on T.
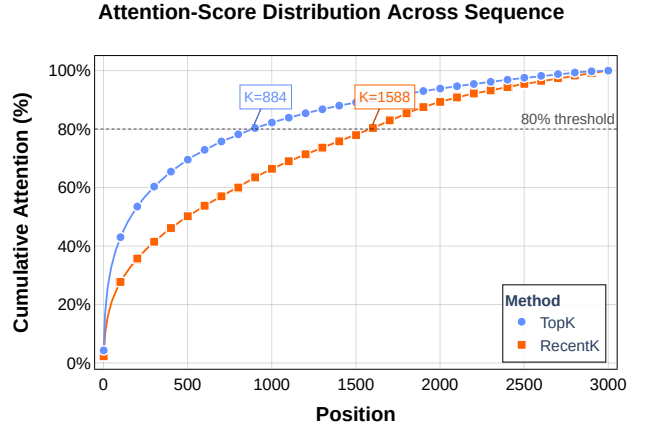

Figure 3 Attention-score distribution across the sequence. The model continues to attend to events throughout the history, supporting the usefulness of long contexts.

6.3.2 Balancing freshness and signal strength

We next examine the composition of the sequence at fixed length. In this setting, user histories combine high-frequency, lower per-event signal actions (ad views) with low-frequency, high-value actions (conversions). We fix $T = 1000$ and vary the allocation between these two sources (Table 2, top).

The balanced mixture of views and conversions performs best; both extremes are clearly suboptimal. Pure-view sequences underperform because they contain many low-signal events. Pure-conversion sequences, while composed of very high-value events, also degrade performance because conversions are temporally sparse: filling a length-1000 sequence with only conversions forces the model to rely on older events that may no longer reflect current intent. Views, by contrast, provide dense and recent coverage. The best-performing allocations combine the high per-event signal of conversions with the temporal freshness provided by

frequent views.

6.3.3 Content-aware scaling: strong content features bend the scaling curve

Finally, we study how feature richness interacts with architectural scaling. In addition to sparse IDs, we introduce dense content embeddings produced by fine-tuned LLaMA models as well as Content Understanding models processing heterogeneous multimodal signals (e.g., text and images) and compare models with and without these features at different depths (Table 2, bottom).

Table 2 Sequence-quality ablations. Top: impact of sequence composition at fixed length $T = 1000$. Bottom: effect of content semantic features at two depths.

Sequence composition ($T = 1000$)		
Allocation (Views / Conv)	**△NE (%)**	
Balanced (500 / 500)	**0.00%**	reference
Conv-heavy (200 / 800)	+0.01%	near-optimal
Pure conversions (0 / 1000)	+0.105%	degraded
Pure views (1000 / 0)	+0.15%	worst
Content features		
Features	**1L model**	**4L model**
Sparse IDs only	+0.06%	-0.01%
Sparse IDs + content embeddings	**0.00%**	**-0.118%**

Two observations stand out. First, in the absence of content features, increasing depth from one to four layers yields only a minor improvement: the 4-layer ID-only model is only slightly better than the 1-layer baseline. This corresponds to a very shallow scaling slope and indicates that additional capacity is largely spent memorizing ID patterns. Second, when LLaMA content embeddings are enabled, the same 4-layer configuration achieves a substantially larger gain, and the relative benefit of content is markedly stronger for the deeper model than for the shallow one.

These results show that strong semantic content features are not a marginal add-on but a prerequisite for effective scaling. The presence of semantic features materially changes the slope of the compute–NE curve: with ID-only inputs, depth and sequence-length scaling quickly exhibit diminishing returns, whereas with content-enriched sequences, the same increases in L and T translate into substantially larger NE gains. In this sense, the scaling law for LLaTTE is inherently *content-aware*; analyzing model size and compute in isolation is insufficient to predict performance.

6.4 Global Compute Scaling

Finally, we aggregate the above experiments to examine global compute scaling. Figure 4 plots relative NE gain versus sequence compute budget $\mathcal{C}$ (measured in sequence FLOPs) on a logarithmic scale.

The results demonstrate that recommendation performance follows a predictable power-law relationship with compute.
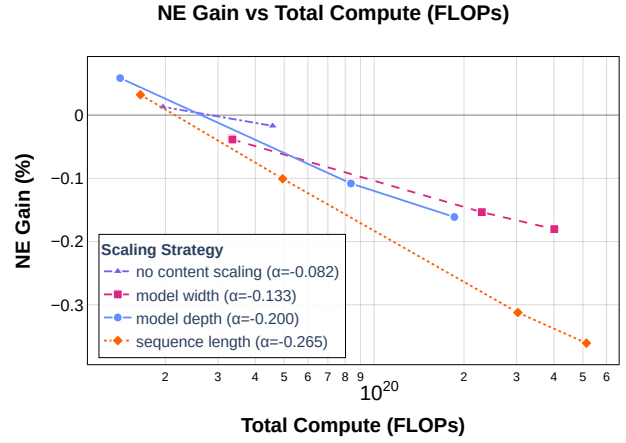

Figure 4 Relative normalized entropy (NE) gain versus training compute (FLOPs, log scale) for different scaling strategies. The slope of each line indicates NE improvement per $10\times$ increase in compute.

We fit a log-linear model to the empirical data:

$$\Delta \mathrm{NE}(\mathcal{C}) = -\alpha \cdot \log_{10} \mathcal{C} + \beta$$

where the scaling coefficient α is determined by the scaling strategy. We observe distinct behaviors for each axis:

- **Sequence Length:** This dimension exhibits the steepest scaling slope. Extending the temporal horizon consistently yields the largest performance improvement per unit of compute, indicating that the model effectively utilizes long-term history. This, however, comes with the additional cost of logging and materializing longer user engagement histories.
- **Model Depth:** Increasing depth provides robust scaling behavior. Once the model width is sufficiently scaled up, adding layers offers a reliable path to improved ranking quality.
- **Model Width:** Width plays a foundational role in the architecture. While the scaling slope is less steep compared to depth or length, sufficient width is essential for maximizing the capacity of the other dimensions.
- **Content Quality:** As shown in Figure 4, the presence of semantic features significantly enhances the scaling laws on all other dimensions. Content-enriched models demonstrate a steep slope compared to their ID-only counterparts (black line), showing that high-quality semantic features are necessary for the model to extract value from increased compute.

These findings establish that sequence-based recommendation is a scalable paradigm that converts compute into predictable performance gains. We leverage this scaling hierarchy in Section 7 to optimize our multi-stage architecture under production constraints.

7

7 Multistage Sequence Model: Towards Maximizing RoI in Production

7.1 Motivation and architecture

Section 6.4 showed that ranking quality continues to improve as we scale depth, and in particular, sequence length. The production ranker, however, serves trillions of requests per day under a strict latency budget, which limits the deployed sequence module to a few layers and a per-source (i.e. engagement type) horizon of roughly $T \approx 400$ events/tokens. To benefit from the favorable scaling curves without violating latency constraints, we adopt a multistage architecture. The latency-constrained **downstream** model remains compact and attends jointly over user sequences and ad/context features. An asynchronous **upstream** user model processes longer histories using the same LLaTTE architecture but with only user-side features, and publishes cached user embeddings that the ranker consumes at request time. This separation introduces a strict information bottleneck, as the upstream encoder must summarize thousands of historical events into a single fixed-size vector (in our production deployment, $d_{\text{transfer}} = 2048$). We study how this fixed-bandwidth bottleneck affects scaling laws.

7.2 Upstream scaling laws

We first characterize the scaling behavior of the upstream user model in isolation. Using the same log-linear fitting procedure as in Section 6.4, we estimate slopes for NE improvement as a function of upstream sequence FLOPs. Table 3 (top) summarizes the comparison between upstream and downstream slopes.

Table 3 Upstream vs downstream scaling comparison.

(a) Slopes α against total model FLOPs ($\mathcal{C}_{\text{full}}$).

	Depth (L)	Width (d)	Seq. length (T)
Downstream α	0.200	0.133	0.265
Upstream α	0.102	0.113	0.116

(b) Slopes α against sequence-only FLOPs ($\mathcal{C}_{\text{seq}}$).

	Depth (L)	Width (d)	Seq. length (T)
Downstream α	0.106	0.091	0.238
Upstream α	0.092	0.102	0.094

(c) Transfer ratios for iso-FLOPs upstream configurations.

	Seq-heavy ($L{=}3, d{=}512, T{=}1000$)	Model-heavy ($L{=}6, d{=}512, T{=}460$)
$\Delta \text{NE}_{\text{up}}$	-0.14%	-0.13%
$\Delta \text{NE}_{\text{down}}$	-0.07%	-0.07%
τ (%)	50	53

Table 3a reports scaling slopes against total model FLOPs. The downstream model exhibits notably steeper slopes across all dimensions. This difference, however, reflects a structural asymmetry: in the downstream ranker, the sequence module accounts for only $\approx 30\%$ of total FLOPs, whereas in the upstream model it accounts for $\approx 90\%$. Scaling the sequence module thus yields a larger relative improvement per total FLOP in the downstream setting.

To isolate the intrinsic scaling efficiency of the sequence module, Table 3b reports slopes against sequence-only FLOPs. This comparison reveals that depth and width scaling efficiency is consistent across both settings. The key difference lies in sequence length: upstream scaling retains only $\approx 50\%$ of the downstream efficiency. This gap arises because the upstream encoder lacks candidate context, forcing it to compress the history into a generic representation rather than performing candidate-aware attention. Consequently, only long-range signals that are universally relevant across candidates survive the bottleneck.

7.3 Transfer efficiency

To quantify the efficiency of our multi-stage architecture, recall the transfer ratio τ defined in Eq. 4. This metric measures the conversion rate of upstream representation quality into downstream ranking accuracy.

For instance, the *Seq-heavy* configuration in Table 3c demonstrates this relationship: upgrading the upstream encoder yields a 0.14% upstream improvement, which translates to a 0.07% improvement in the downstream ranker, corresponding to a transfer ratio of $\tau \approx 50\%$.

Benchmarking Transfer Efficiency. Transferring gains from asynchronous upstream models to online rankers is inherently lossy. Several structural factors typically limit transfer efficiency to the 25%–30% range: the *capacity gap* between massive upstream encoders and compact downstream rankers, the *staleness* introduced by asynchronous inference, and the *information bottleneck* imposed by compressing user histories into fixed-size user embeddings. Against this backdrop, the $\approx 50\%$ transfer ratio observed in our experiments is significant. It indicates that the high-level intent signals captured by scaling the sequence encoder are robust to compression and temporal delays, retaining substantial predictive value despite the aggressive compression and separation from the online scoring context.

Architecture Robustness. To determine if specific architectural choices affect this efficiency, we compare two upstream configurations with matched compute budgets (≈ 12 GFLOPs/sample) representing different scaling priorities:

- **Sequence-heavy**: $L = 3, d = 512, T = 1000$
- **Model-heavy**: $L = 6, d = 512, T = 460$

As shown in Table 3 (bottom), both models achieve similar upstream gains (-0.14% vs -0.13%) and, crucially, identical downstream gains (-0.07%). This indicates that for a fixed compute budget, the architecture is robust to the specific

allocation between depth and sequence length. The total compute of the upstream model determines the downstream performance, validating that we can flexibly trade off history length for model capacity without degrading the transfer ratio.

7.4 Implications for compute allocation

The combined downstream and upstream observations yield a simple policy:

- **Downstream online ranker:** Allocate the latency budget to short sequence lengths and shallow depths, supported by sufficient width and rich content features (sequence lengths up to $T \approx 400$).
- **Asynchronous upstream user model:** Use the relaxed latency budget to scale total sequence-modeling compute. Results indicate that downstream performance is driven primarily by the total upstream compute budget rather than the specific allocation between depth and length. Consequently, we deploy upstream models with a sequence compute budget $45\times$ larger than that of the online ranker.

This two-stage asymmetric strategy lets us continue following the scaling frontier identified in Section 6.4 after the latency-constrained ranker has exhausted its local budget, turning additional offline compute into predictable online gains.

8 Production Deployment

8.1 Asynchronous embedding service with online LLaTTE

In production, we deploy a two-stage LLaTTE architecture. The *downstream* ranking model continues to run a compact LLaTTE module online, attending over short user histories (per-source horizon capped at $T \approx 400$) together with ad and context features, under a strict per-request latency budget at trillion-request scale. This online LLaTTE model captures fresh user intent signals and leverages ad-specific interactions, but is intentionally much smaller than the models investigated in the scaling study presented in Section 6.4.

To exploit bigger sequence models without impacting latency, we introduce an *asynchronous embedding service* that hosts the *upstream* user understanding LLaTTE model. Embedding updates are not computed per request; instead, they are triggered on high-value user events (primarily user conversions). Triggered events are processed on a dedicated cluster of H100 GPU hosts using deeper and longer LLaTTE models optimized for high-throughput transformer inference. Representing the largest user model deployment at Meta, these upstream encoders operate only on user-side features, generate user representations (embeddings), and write their compressed representations to a feature store. At request time, the downstream ranking models read these embeddings as dense features and utilize them in the online downstream LLaTTE ranking model.

8.2 Latency and online gains

Offloading heavy sequence modeling to the asynchronous embedding service keeps the additional cost on the ranking path to a single feature lookup. The online downstream LLaTTE model remains conservative in design (depth and sequence length). We observe no measurable change in P99 ranking latency compared to the baseline without upstream LLaTTE user embeddings. The extra FLOPs from the larger upstream LLaTTE models are absorbed by the H100 cluster, which operates at much lower QPS and is heavily batched.

Across multiple large-scale A/B tests, the combination of the compact online LLaTTE and the upstream LLaTTE user embeddings delivered approximately **0.25%** NE reduction on our flagship ads ranker, corresponding to a 4.3% conversion uplift on Facebook Feed and Reels, a business impact on the order of hundreds of millions of dollars in annual revenue. This validates the proposed two-stage scaling strategy as an efficient way to convert additional sequence-modeling compute into production value under strict serving constraints.

9 Conclusion & Future Work

In this work, we propose the LLaTTE paradigm, which significantly scales up sequence learning in recommender systems. By allocating the majority of computational resources to sequence modeling, we achieve predictable and robust scaling behavior. We systematically analyze scaling across standard dimensions (model depth and width) as well as less explored factors (sequence length, composition and richness), demonstrating that optimal scaling requires balancing all these factors simultaneously.

To maximize production impact, we develop a multistage modeling and deployment strategy: a computationally expensive model trained on user-only features that runs offline and infrequently, while effectively transferring these gains to the lightweight online production model.

Our work was developed concurrently with other notable industry advances in sequence modeling for recommender systems Zhang et al. (2025); Deng et al. (2025). These efforts collectively demonstrate the rise of sequence modeling in large-scale recommendation systems. Moving forward, we plan to explore efficient long-context kernels, reinforcement learning, scalable infrastructure solutions, and the upper bounds of scaling laws – as we stand at the cusp of the LLM-scale era for recommender systems.

References

Zheng Chai, Qin Ren, Xijun Xiao, Huizhi Yang, Bo Han, Sijun Zhang, Di Chen, Hui Lu, Wenlin Zhao, Lele Yu, Xionghang Xie, Shiru Ren, Xiang Sun, Yaocheng Tan, Peng Xu, Yuchao Zheng, and Di Wu. 2025. LONGER: Scaling Up Long Sequence Modeling in Industrial Recommenders. arXiv:2505.04421 [cs.IR] https://arxiv.org/abs/2505.04421

Jianxin Chang, Chenbin Zhang, Zhiyi Fu, Xiaoxue Zang, Lin Guan, Jing Lu, Yiqun Hui, Dewei Leng, Yanan Niu, Yang Song, and Kun Gai. 2023. TWIN: TWo-stage Interest Network for Lifelong User Behavior Modeling in CTR Prediction at Kuaishou. In *Proceedings of the 29th ACM SIGKDD Conference on Knowledge Discovery and Data Mining*. https://arxiv.org/abs/2302.02352

Junyi Chen, Lu Chi, Bingyue Peng, and Zehuan Yuan. 2024. HLLM: Enhancing Sequential Recommendations via Hierarchical Large Language Models for Item and User Modeling. arXiv:2409.12740 [cs.IR] https://arxiv.org/abs/2409.12740

Qiwei Chen, Huan Zhao, Wei Li, Pipei Huang, and Wenwu Ou. 2019. Behavior Sequence Transformer for E-commerce Recommendation in Alibaba. arXiv:1905.06874 [cs.IR] https://arxiv.org/abs/1905.06874

Tri Dao, Daniel Y. Fu, Stefano Ermon, Atri Rudra, and Christopher Ré. 2022. FlashAttention: Fast and Memory-Efficient Exact Attention with IO-Awareness. arXiv:2205.14135 [cs.LG] https://arxiv.org/abs/2205.14135

DeepSeek-AI. 2024. DeepSeek-V2: A Strong, Economical, and Efficient Mixture-of-Experts Language Model. arXiv:2405.04434 [cs.CL] https://arxiv.org/abs/2405.04434

Jiaxin Deng, Shiyao Wang, Kuo Cai, Lejian Ren, Qigen Hu, Weifeng Ding, Qiang Luo, and Guorui Zhou. 2025. OneRec: Unifying Retrieve and Rank with Generative Recommender and Iterative Preference Alignment. arXiv:2502.18965 [cs.IR] https://arxiv.org/abs/2502.18965

Tim Donkers, Benedikt Loepp, and Jürgen Ziegler. 2017. Sequential User-based Recurrent Neural Network Recommendations. In *Proceedings of the Eleventh ACM Conference on Recommender Systems* (Como, Italy) *(RecSys '17)*. Association for Computing Machinery, New York, NY, USA, 152–160. doi:10.1145/3109859.3109877

Huifeng Guo, Ruiming Tang, Yunming Ye, Zhenguo Li, and Xiuqiang He. 2017. DeepFM: A Factorization-Machine based Neural Network for CTR Prediction. *CoRR* abs/1703.04247 (2017). arXiv:1703.04247 http://arxiv.org/abs/1703.04247

Balázs Hidasi, Alexandros Karatzoglou, Linas Baltrunas, and Domonkos Tikk. 2016. Session-based Recommendations with Recurrent Neural Networks. arXiv:1511.06939 [cs.LG] https://arxiv.org/abs/1511.06939

Andrew Jaegle, Felix Gimeno, Andrew Brock, Andrew Zisserman, Oriol Vinyals, and Joao Carreira. 2021. Perceiver: General Perception with Iterative Attention. arXiv:2103.03206 [cs.CV] https://arxiv.org/abs/2103.03206

Wang-Cheng Kang and Julian McAuley. 2018. Self-Attentive Sequential Recommendation. arXiv:1808.09781 [cs.IR] https://arxiv.org/abs/1808.09781

Jared Kaplan, Sam McCandlish, Tom Henighan, Tom B. Brown, Benjamin Chess, Rewon Child, Scott Gray, Alec Radford, Jeffrey Wu, and Dario Amodei. 2020. Scaling Laws for Neural Language Models. arXiv:2001.08361 [cs.LG] https://arxiv.org/abs/2001.08361

Maxim Naumov, Dheevatsa Mudigere, Hao-Jun Michael Shi, Jianyu Huang, Narayanan Sundaraman, Jongsoo Park, Xiaodong Wang, Udit Gupta, Carole-Jean Wu, Alisson G. Azzolini, Dmytro Dzhulgakov, Andrey Mallevich, Ilia Cherniavskii, Yinghai Lu, Raghuraman Krishnamoorthi, Ansha Yu, Volodymyr Kondratenko, Stephanie Pereira, Xianjie Chen, Wenlin Chen, Vijay Rao, Bill Jia, Liang Xiong, and Misha Smelyanskiy. 2019. Deep Learning Recommendation Model for Personalization and Recommendation Systems. *CoRR* abs/1906.00091 (2019). arXiv:1906.00091 http://arxiv.org/abs/1906.00091

Nikil Pancha, Andrew Zhai, Jure Leskovec, and Charles Rosenberg. 2022. PinnerFormer: Sequence Modeling for User Representation at Pinterest. arXiv:2205.04507 [cs.LG] https://arxiv.org/abs/2205.04507

Qi Pi, Xiaoqiang Zhu, Guorui Zhou, Yujing Zhang, Zhe Wang, Lejian Ren, Ying Fan, and Kun Gai. 2020. Search-based User Interest Modeling with Lifelong Sequential Behavior Data for Click-Through Rate Prediction. In *Proceedings of the 29th ACM International Conference on Information and Knowledge Management*. https://arxiv.org/abs/2006.05639

Noam Shazeer. 2019. Fast Transformer Decoding: One Write-Head is All You Need. arXiv:1911.02150 [cs.NE] https://arxiv.org/abs/1911.02150

Zihua Si, Lin Guan, ZhongXiang Sun, Xiaoxue Zang, Jing Lu, Yiqun Hui, Xingchao Cao, Zeyu Yang, Yichen Zheng, Dewei Leng, Kai Zheng, Chenbin Zhang, Yanan Niu, Yang Song, and Kun Gai. 2024. TWIN V2: Scaling Ultra-Long User Behavior Sequence Modeling for Enhanced CTR Prediction at Kuaishou. In *Proceedings of the 33rd ACM International Conference on Information and Knowledge Management*. https://arxiv.org/abs/2407.16357

Fei Sun, Jun Liu, Jian Wu, Changhua Pei, Xiao Lin, Wenwu Ou, and Peng Jiang. 2019. BERT4Rec: Sequential Recommendation with Bidirectional Encoder Representations from Transformer. *CoRR* abs/1904.06690 (2019). arXiv:1904.06690 http://arxiv.org/abs/1904.06690

Ruoxi Wang, Bin Fu, Gang Fu, and Mingliang Wang. 2017. Deep & Cross Network for Ad Click Predictions. *CoRR* abs/1708.05123 (2017). arXiv:1708.05123 http://arxiv.org/abs/1708.05123

Ruoxi Wang, Rakesh Shivanna, Derek Cheng, Sagar Jain, Dong Lin, Lichan Hong, and Ed Chi. 2021. DCN V2: Improved Deep & Cross Network and Practical Lessons for Web-scale Learning to Rank Systems. In *Proceedings of the Web Conference 2021 (WWW '21)*. ACM, 1785–1797. doi:10.1145/3442381.3450078

Xue Xia, Pong Eksombatchai, Nikil Pancha, Dhruvil Deven Badani, Po-Wei Wang, Neng Gu, Saurabh Vishwas Joshi, Nazanin Farahpour, Zhiyuan Zhang, and Andrew Zhai. 2023. TransAct: Transformer-based Realtime User Action Model for Recommendation at Pinterest. In *Proceedings of the 29th ACM SIGKDD Conference on Knowledge Discovery and Data Mining (KDD '23)*. ACM, 5249–5259. doi:10.1145/3580305.3599918

Xue Xia, Saurabh Vishwas Joshi, Kousik Rajesh, Kangnan Li, Yangyi Lu, Nikil Pancha, Dhruvil Deven Badani, Jiajing Xu, and Pong Eksombatchai. 2025. TransAct V2: Lifelong User Action Sequence Modeling on Pinterest Recommendation. arXiv:2506.02267 [cs.IR] https://arxiv.org/abs/2506.02267

Zhichen Zeng, Xiaolong Liu, Mengyue Hang, Xiaoyi Liu, Qinghai Zhou, Chaofei Yang, Yiqun Liu, Yichen Ruan, Laming Chen, Yuxin Chen, Yujia Hao, Jiaqi Xu, Jade Nie, Xi Liu, Buyun Zhang, Wei Wen, Siyang Yuan, Hang Yin, Xin Zhang, Kai Wang, Wen-Yen Chen, Yiping Han, Huayu Li, Chunzhi Yang, Bo Long, Philip S. Yu, Hanghang Tong, and Jiyan Yang. 2025. InterFormer: Effective Heterogeneous Interaction Learning for Click-Through Rate Prediction. arXiv:2411.09852 [cs.IR] https://arxiv.org/abs/2411.09852

Jiaqi Zhai, Lucy Liao, Xing Liu, Yueming Wang, Rui Li, Xuan Cao, Leon Gao, Zhaojie Gong, Fangda Gu, Michael He, Yinghai Lu, and Yu Shi. 2024. Actions Speak Louder than Words: Trillion-Parameter Sequential Transducers for Generative Recommendations. arXiv:2402.17152 [cs.LG] https://arxiv.org/abs/2402.17152

Buyun Zhang, Liang Luo, Yuxin Chen, Jade Nie, Xi Liu, Daifeng Guo, Yanli Zhao, Shen Li, Yuchen Hao, Yantao Yao, Guna Lakshminarayanan, Ellie Dingqiao Wen, Jongsoo Park, Maxim Naumov, and Wenlin Chen. 2024b. Wukong: Towards a Scaling Law for Large-Scale Recommendation. arXiv:2403.02545 [cs.LG] https://arxiv.org/abs/2403.02545

Buyun Zhang, Liang Luo, Xi Liu, Jay Li, Zeliang Chen, Weilin Zhang, Xiaohan Wei, Yuchen Hao, Michael Tsang, Wenjun Wang, Yang Liu, Huayu Li, Yasmine Badr, Jongsoo Park, Jiyan Yang, Dheevatsa Mudigere, and Ellie Wen. 2022. DHEN: A Deep and Hierarchical Ensemble Network for Large-Scale Click-Through Rate Prediction. arXiv:2203.11014 [cs.IR] https://arxiv.org/abs/2203.11014

Biao Zhang and Rico Sennrich. 2019. Root Mean Square Layer Normalization. arXiv:1910.07467 [cs.LG] https://arxiv.org/abs/1910.07467

Wei Zhang, Dai Li, Chen Liang, Fang Zhou, Zhongke Zhang, Xuewei Wang, Ru Li, Yi Zhou, Yaning Huang, Dong Liang, Kai Wang, Zhangyuan Wang, Zhengxing Chen, Fenggang Wu, Minghai Chen, Huayu Li, Yunnan Wu, Zhan Shu, Mindi Yuan, and Sri Reddy. 2024a. Scaling User Modeling: Large-scale Online User Representations for Ads Personalization in Meta. In *Companion Proceedings of the ACM Web Conference 2024 (WWW '24)*. ACM, 47–55. doi:10.1145/3589335.3648301

Zhaoqi Zhang, Haolei Pei, Jun Guo, Tianyu Wang, Yufei Feng, Hui Sun, Shaowei Liu, and Aixin Sun. 2025. OneTrans: Unified Feature Interaction and Sequence Modeling with One Transformer in Industrial Recommender. arXiv:2510.26104 [cs.IR] https://arxiv.org/abs/2510.26104

Guorui Zhou, Na Mou, Ying Fan, Qi Pi, Weijie Bian, Chang Zhou, Xiaoqiang Zhu, and Kun Gai. 2019. Deep Interest Evolution Network for Click-Through Rate Prediction. In *Proceedings of the AAAI Conference on Artificial Intelligence*, Vol. 33. 5941–5948. https://arxiv.org/abs/1809.03672

Guorui Zhou, Chengru Song, Xiaoqiang Zhu, Ying Fan, Han Zhu, Xiao Ma, Yanghui Yan, Junqi Jin, Han Li, and Kun Gai. 2018. Deep Interest Network for Click-Through Rate Prediction. In *Proceedings of the 24th ACM SIGKDD International Conference on Knowledge Discovery and Data Mining*. https://arxiv.org/abs/1706.06978

Kun Zhou, Hui Wang, Wayne Xin Zhao, Yutao Zhu, Sirui Wang, Fuzheng Zhang, Zhongyuan Wang, and Ji-Rong Wen. 2020. S3-Rec: Self-Supervised Learning for Sequential Recommendation with Mutual Information Maximization. In *Proceedings of the 29th ACM International Conference on Information & Knowledge Management (CIKM '20)*. ACM, 1893–1902. doi:10.1145/3340531.3411954

A LLaTTE Architecture Details

A.1 Non-Sequence Module

Let $\mathcal{E} : \mathcal{V} \to \mathbb{R}^{d_e}$ denote the embedding lookup for sparse categorical features. We construct the initial non-sequence representation by concatenating embedded sparse features, dense features, float features, and sequence summaries:

$$\mathbf{h}^{(0)} = \text{Concat}\Big(\mathcal{E}(\mathbf{x}_{\text{sparse}}),\ \mathbf{x}_{\text{dense}},\ \mathbf{x}_{\text{float}},\ \{\mathbf{z}_{\text{seq}}^{(k)}\}_{k=1}^{m_{\text{seq}}}\Big) \in \mathbb{R}^{d_0}. \tag{5}$$

We then apply L_{NS} layers of a feature-interaction network:

$$\mathbf{h}^{(\ell)} = \text{NonSeq}_\ell(\mathbf{h}^{(\ell-1)}), \quad \ell = 1, \ldots, L_{\text{NS}}, \tag{6}$$

yielding

$$\mathbf{z} = \mathbf{h}^{(L_{\text{NS}})} \in \mathbb{R}^d. \tag{7}$$

In production, NonSeq_ℓ is instantiated with a DCN/DeepFM/DLRM-style architecture Guo et al. (2017); Naumov et al. (2019); Wang et al. (2017, 2021); Zhang et al. (2024b).

A.2 Sequence Module

A.2.1 Action Embeddings

Let $S_u = \{a_1, a_2, \ldots, a_T\}$ be the temporally ordered sequence of actions, oldest first. Each action $a_t = (\tau_t, \text{type}_t, \text{item}_t, \text{surface}_t, \text{meta}_t)$ is embedded and projected into a token:

$$\mathbf{x}_t = \text{MLP}_{\text{act}}\Big(\mathcal{E}_{\text{type}}(\text{type}_t),\ \mathcal{E}_{\text{item}}(\text{item}_t),$$

$$\mathcal{E}_{\text{surface}}(\text{surface}_t),\ \mathcal{E}_{\text{time}}(\tau_t),\ \mathcal{E}_{\text{meta}}(\text{meta}_t)\Big) \in \mathbb{R}^d$$

forming

$$\mathbf{X}_{\text{seq}} = [\mathbf{x}_1; \mathbf{x}_2; \ldots; \mathbf{x}_T] \in \mathbb{R}^{T \times d}. \tag{8}$$

We apply additive timestamp encodings to a subset of hidden dimensions.

A.2.2 Query Tokens and Fusion

We introduce n_q query tokens $\mathbf{Q} \in \mathbb{R}^{n_q \times d}$ that summarize the user–ad request. Depending on the stage, these tokens may encode candidate ad features, request context, user-level features, and learned seed tokens Jaegle et al. (2021). We concatenate sequence and query tokens:

$$\mathbf{X}_{\text{input}} = \text{Concat}(\mathbf{X}_{\text{seq}}, \mathbf{Q}) \in \mathbb{R}^{(T+n_q) \times d}, \tag{9}$$

and feed $\mathbf{X}_{\text{input}}$ into the transformer.

A.2.3 Transformer Layers and Pyramidal Schedule

We apply an L-layer causal transformer with Multi-head Latent Attention (MLA) DeepSeek-AI (2024) and RMS normalization Zhang and Sennrich (2019). Let $\mathbf{R}^{(0)} = \mathbf{X}_{\text{input}}$. For layer ℓ:

$$\mathbf{Z}^{(\ell)} = \text{RMSNorm}\big(\mathbf{R}^{(\ell)} + \text{MLA}(\mathbf{R}^{(\ell)})\big), \qquad (10)$$

$$\mathbf{X}^{(\ell)} = \text{RMSNorm}\big(\mathbf{Z}^{(\ell)} + \text{FFN}(\mathbf{Z}^{(\ell)})\big). \qquad (11)$$

Following Zhang et al. (2025), we use an adaptive pyramidal schedule over the temporal dimension. If $\mathbf{X}^{(\ell)} \in \mathbb{R}^{(T_\ell + n_q) \times d}$, the next layer operates on

$$\mathbf{R}^{(\ell+1)} = \mathbf{X}^{(\ell)}[:, -T_{\ell+1}:, :] \in \mathbb{R}^{T_{\ell+1} \times d}, \qquad (12)$$

where $T_{\ell+1} \leq T_\ell$. This progressively trims older tokens, reducing attention cost $\mathcal{O}(T_{\ell+1} T_\ell d)$ and FFN cost $\mathcal{O}(T_{\ell+1} d^2)$.

We use three regimes:

- **Full self-attention** $(T_\ell = T + n_q)$: all sequence and query tokens are retained.
- **Pyramidal attention** $(n_q < T_\ell < T + n_q)$: query tokens plus the $m = T_\ell - n_q$ most recent actions.
- **Cross-attention** $(T_\ell = n_q)$: only query tokens are retained; used in the final layer.

Offline (upstream) models typically use more layers with full self-attention (except the final cross-attention layer). Online ranking models use more aggressive pyramidal trimming in early layers before the final cross-attention layer.

A.2.4 Sequence Summaries

The final layer outputs $\mathbf{Z}_{\text{raw}}$ at the query-token positions. We project these into one or more fixed-size sequence summaries:

$$\mathbf{z}_{\text{seq}}^{(k)} = \text{LoRAMLP}_k\big(\text{Flatten}(\mathbf{Z}_{\text{raw}})\big) \in \mathbf{R}^{d_{\text{seq}}}, \qquad (13)$$

where each LoRAMLP_k is a low-rank adapted MLP.

A.3 Multi-head Latent Attention

For completeness, we include the MLA parameterization. For h heads, given input $\mathbf{X} \in \mathbf{R}^{h \times d}$:

$$\mathbf{K}, \mathbf{V} \in \mathbb{R}^{T \times h \times d_k} = \text{split}\big(\text{RMSNorm}(\mathbf{X}\mathbf{W}_{\text{down}}^{KV})\mathbf{W}_{\text{up}}^{KV}\big) \qquad (14)$$

$$\mathbf{Q} \in \mathbb{R}^{T \times h \times d_k} = \text{RMSNorm}(\mathbf{X}\mathbf{W}_{\text{down}}^{Q})\mathbf{W}_{\text{up}}^{Q} \qquad (15)$$

$$\text{MLA}(\mathbf{X}) \in \mathbb{R}^{T \times d} = \text{softmax}\left(\frac{\mathbf{Q}\mathbf{K}^{\top}}{\sqrt{d_k}}\right)\mathbf{V}\mathbf{W}_{\text{out}} \qquad (16)$$

A key observation is that consecutive linear projections can be algebraically absorbed into single matrices. Specifically:

- the $\mathbf{W}_{\text{up}}^{Q}$ and the $\mathbf{W}_{\text{up}}^{KV\top}$ on $\mathbf{K}^{\top}$ can be fused
- the $\mathbf{W}_{\text{up}}^{KV}$ on Q can be absorbed into $\mathbf{W}_{\text{out}}$

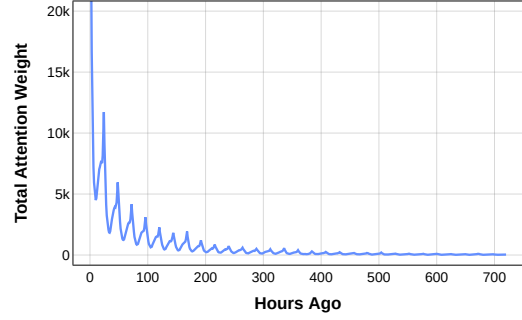**Total Attention Weight Distribution Across Time**

Figure 5 Total attention weight distributed to event tokens bucketized by hours prior to the user request.

This simplification reveals that MLA is mathematically equivalent to Multi-Query Attention (MQA) Shazeer (2019) on the latent space, where queries are projected to multiple heads while key-value representations remain shared in the compressed latent space. The reformulated equations are as follows:

$$\mathbf{Q}_{\text{latent}} \in \mathbb{R}^{T \times h \times d_c} = \text{RMSNorm}(\mathbf{X}\mathbf{W}_{\text{down}}^{Q}) \qquad (17)$$

$$\mathbf{KV}_{\text{latent}} \in \mathbb{R}^{T \times d_c} = \text{RMSNorm}(\mathbf{X}\mathbf{W}_{\text{down}}^{KV}) \qquad (18)$$

$$\text{MLA}(\mathbf{X}) \in \mathbb{R}^{T \times d} = \text{softmax}\left(\frac{\mathbf{Q}_{\text{latent}}\mathbf{W}^{QK}\mathbf{KV}_{\text{latent}}^{\top}}{\sqrt{d_c}}\right)$$
$$\cdot \mathbf{KV}_{\text{latent}}\mathbf{W}_{\text{out}}^{V} \qquad (19)$$

A.4 Attention Weight Distribution

We studied the attention weight distribution P

$$P = \text{softmax}\left(\frac{\mathbf{Q}\mathbf{K}^{\top}}{\sqrt{d_k}}\right) \qquad (20)$$

To enhance the visualization of attention weights, we reduced both the number of query tokens and the number of attention heads in a single-layer transformer LLaTTE backbone. We extracted the attention probabilities of each query token with respect to the entire user sequence and aggregated these probabilities across a sufficient number of samples from diverse user requests.

Our analysis reveals that the model allocates a greater proportion of its attention to the most recent events. However, it continues to assign non-negligible probabilities to longer-term history, indicating that the model does not disregard earlier events entirely Figure 3. Interestingly, we also examined the cumulative attention weight by selecting topK event tokens instead most recent k tokens, which present the theoretical maximum cumulative attention weight achievable by selecting k tokens.

Additionally, we identified notable seasonality patterns at the daily level. As shown in Figure 5 and Figure 6, the
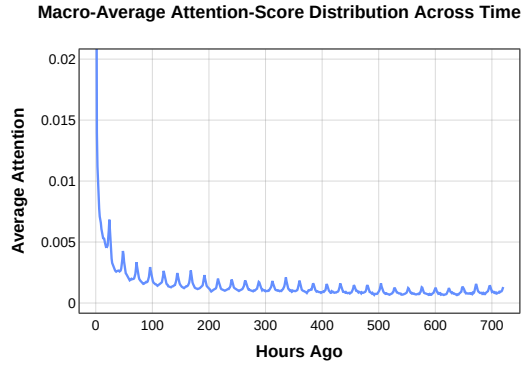
Figure 6 Average attention weight per event by hours prior to the user request.

attention weight spikes occur at sharp 24-hour intervals. This suggests that individual users tend to exhibit recurring interests and behaviors at similar times of day.

While these findings are consistent with our intuitions, we recognize that a more granular understanding of user behavior in relation to behavioral sequences remains an open area for exploration. We present these preliminary results to encourage further research and contributions from the broader community.

B   Acknowledgments